

potential radius over density radius by about 1.35 fermis, independent of atomic weight. This corresponds to somewhat larger difference in the half density radii. While the closeness of this theoretical estimate to the experimental result might be fortuitous, it is encouraging to note that the results of the phenomenological theory can be tested by direct experiments. The non-linearity effect of Wilets should not be seen by pions,

and this has been experimentally verified by Cool *et al.*³³ Drell³⁶ has also suggested recently that the part of the difference which arises from finite range of nuclear forces should approach zero for incident protons or neutrons of several Bev energies. No clear-cut measurements of the nuclear potential radius by elastic scattering are available as yet in this region of interest, however.

Mirror Nuclei Determinations of Nuclear Size

O. KOFOED-HANSEN

Danish Atomic Energy Commission, Risø, Denmark

INTRODUCTION

IT was suggested by Bethe¹ that the differences in Coulomb energies between adjacent pairs of mirror nuclei be interpreted as the Coulomb energy difference for homogeneously charged spheres of the appropriate charges. The resultant radius of the sphere is then a measure of the nuclear radius or more precisely the radius R of the equivalent sphere

$$R^2 = (5/3) \langle r^2 \rangle_{Av}. \tag{1}$$

The classical Coulomb energy of a homogeneously charged sphere is given as

$$E_c = \frac{3}{5} (e^2 Z^2 / R), \tag{2}$$

where R is the radius and eZ is the charge. The Coulomb energy difference between nuclei of the same radius but charge values Z and $Z+1$ is consequently given by

$$E_c(Z+1, Z) = 0.6 \frac{2Z+1}{R} e^2. \tag{3}$$

This formula includes a term $E(1,0)$ which would give rise to a radius for the proton from the proton self-energy. This point lies outside the scope of the present paper and we shall prefer to subtract this, energy, i.e., the $n-p$ mass difference in all subsequent considerations i.e., we shall use instead the formula,

$$E_c(Z+1, Z) = 0.6 \frac{2Z+1}{R} e^2 - E_c(1,0), \tag{4}$$

together with the definitions of Coulomb energies

$$\left. \begin{aligned} E_c &= E^{\max} + 1.804 \text{ Mev for } \beta^+ \text{ decay} \\ E_c &= E^{\max} + 0.782 \text{ Mev for } K \text{ capture} \end{aligned} \right\}, \tag{5}$$

and $E_c = E^{\max} - 0.782 \text{ Mev for } \beta^- \text{ decay}$

whereby (4) and (5) are mutually consistent. Also (4) is in better agreement with shell model ideas than the expression,

$$E_c = -\frac{3 e^2 Z(Z-1)}{5 R}, \tag{2a}$$

often applied in order to take into account the fact that charge is applied in integral units of e .

Since Bethe's first application of this method it has been used several times² and calculations have also been made using quantum mechanical descriptions.³⁻⁷ This article reviews the empirical results and gives a description of the methods for interpretation.

INCLUSION OF THE $4n+2$ NUCLEI

Making the assumption that

$$R = r_0 A^{\frac{1}{3}}, \tag{6}$$

and furthermore assuming a negligible variation in r_0 from A to $A \pm 1$, we may also utilize the data from the relative position of the $T=1$ states in the $4n+2$ nuclei for the determination of mirror nuclei Coulomb energies. We consider the change in E_c as being due to a volume change only caused by the addition or subtraction of one neutron, i.e., for a $4n+2$ Coulomb energy defined by (5) and obtained for a $T=1$ transition we

² E. P. Wigner, Phys. Rev. **56**, 519 (1939); White, Creutz, Delsasso, and Wilson, Phys. Rev. **59**, 63 (1941); E. Feenberg and G. Goertzel, Phys. Rev. **70**, 597 (1946); R. R. Wilson, Phys. Rev. **88**, 350 (1952); D. C. Peaslee, Phys. Rev. **95**, 717 (1954).

³ L. N. Cooper and E. M. Henley, Phys. Rev. **92**, 801 (1953).

⁴ B. G. Jancovici, Phys. Rev. **95**, 717 (1954).

⁵ B. C. Carlson and I. Talmi, Phys. Rev. **96**, 436 (1954).

⁶ O. Kofoed-Hansen, Nuclear Phys. **2**, 441 (1956-1957).

⁷ P. C. Sood and A. E. S. Green, Nuclear Phys. (to be published).

¹ H. A. Bethe, Phys. Rev. **54**, 436 (1938).

TABLE I. Mass number and measured Coulomb energies for mirror transitions, are given as deduced from β -decay data and Q values both for mirror transitions and for $4n+2$ nuclei according to Eqs. (7) and (8) and Table II.

A	E_c (Mev)	$\frac{1}{2}A^{\frac{2}{3}}$
1	0.000	0.500
3	0.764 ± 0.001	1.040
5	0.835 ± 0.050	1.462
7	1.646 ± 0.002	1.830
9	2.032 ± 0.006	2.163
11	2.761 ± 0.003	2.473
13	3.006 ± 0.005	2.764
15	3.539 ± 0.006	3.041
17	3.550 ± 0.006	3.306
19	4.027 ± 0.008	3.560
21	4.266 ± 0.006	3.806
23	4.841 ± 0.010	4.044
25	5.062 ± 0.008	4.275
27	5.584 ± 0.010	4.500
29	5.749 ± 0.010	4.720
31	6.220 ± 0.060	4.934
33	6.360 ± 0.030	5.144
35	6.760 ± 0.040	5.350
37	6.920 ± 0.110	5.552
39	7.294 ± 0.030	5.750
41	6.740 ± 0.050	5.945

plot the observed value E_c^{4n+2} as

$$E_c^{4n+2}(Z=2n+2, Z=2n+1) \left[\frac{4n+2}{4n+3} \right]^{\frac{2}{3}} \quad (7)$$

at

$$Z^1/A^{\frac{1}{3}} = \frac{1}{2}[4n+3]^{\frac{2}{3}}$$

if the transition is of the type $Z=2n+2 \rightleftharpoons Z=2n+1$, and as

$$E_c^{4n+2}(Z=2n+1, Z=2n) \left[\frac{4n+2}{4n+1} \right]^{\frac{2}{3}} \quad (8)$$

at

$$Z^1/A^{\frac{1}{3}} = \frac{1}{2}[4n+1]^{\frac{2}{3}}$$

if the transition is of the type $Z=2n+1 \rightleftharpoons Z=2n$. This should then give results comparable with mirror transitions on plotting the latter as a function of

$$Z^1/A^{\frac{1}{3}} = \frac{1}{2} \frac{2Z+1}{A^{\frac{1}{3}}} = \frac{1}{2} A^{\frac{2}{3}} \quad (9)$$

which is the natural procedure when one wants to compare with the expressions (4) and (6).

Small corrections to this procedure occur when more detailed theoretical considerations are applied. These

TABLE II. Comparison of measured mirror nuclei E_c values with those inferred from $4n+2$ nuclei according to Eqs. (7) and (8) and in the last column including the correction from Eq. (19).

A	A_{4n+2}	E_c mirror Mev	$E_c^{4n+2} \left(\frac{A_{4n+2}^{\frac{2}{3}}}{A_{\text{mirror}}^{\frac{2}{3}}} \right)$ Mev	$E_c^{4n+2} \left(\frac{A_{4n+2}^{\frac{2}{3}} B_{\text{mirror}}}{A_{\text{mirror}}^{\frac{2}{3}} B_{4n+2}} \right)$ Mev
11	10	2.763 ± 0.003	2.631 ± 0.030	2.653 ± 0.030
13	14	3.006 ± 0.005	3.014 ± 0.005	2.999 ± 0.005
15	14	3.537 ± 0.006	3.532 ± 0.014	3.547 ± 0.014
21	22	4.300 ± 0.030	4.281 ± 0.006	4.245 ± 0.006
25	26	5.084 ± 0.025	5.071 ± 0.008	5.044 ± 0.008

corrections are taken into account as discussed in connection with Eq. (19).

EXPERIMENTAL RESULTS

Experimental values for mirror nuclei β -decay energies and/or Q values are given in Table I. A value is given for E_c at each value of $Z=2n+1$. In these values are also included $4n+2$ nuclei data interpreted as described in Eqs. (7) and (8). New results have been added to the data which have been summarized previously.⁸

Thus, the $O^{14}-N^{14}$ decay has been investigated by Bromley *et al.*⁹ by a study of the Q value for the reaction $C^{12}(\text{He}^3n)O^{14}$. By comparison with other Q values in this mass region the value $E^{\text{max}} = 1.810 \pm 0.008$ Mev is derived. This value is lower than the β -spectroscopic value given previously but leads to a considerably more acceptable ft value. The new value is also adopted by Gerhart who carried out the β -spectroscopic investigation.¹⁰

The most recent evidence on the $4n+2$ nuclei is given by Gerhart.¹⁰ To this we add a few remarks on the most uncertain E^{max} determinations.

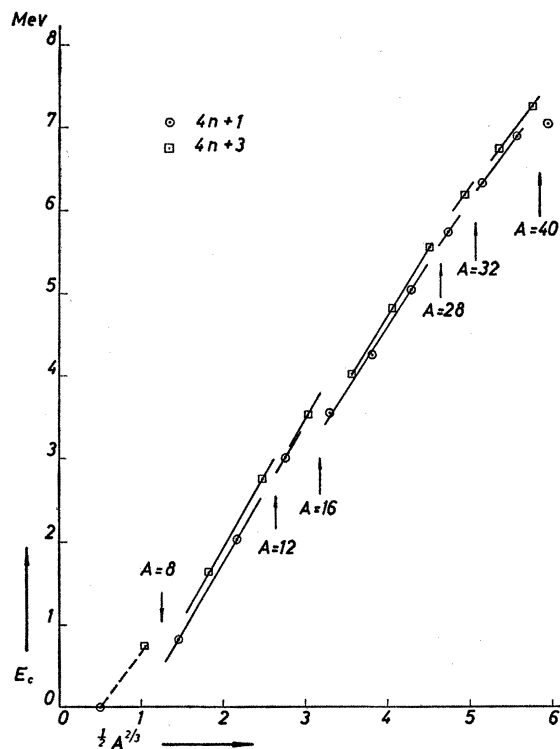


Fig. 1. Experimental Coulomb energy differences as a function of $\frac{1}{2}A^{\frac{2}{3}}$. Individual lines are drawn inside each subshell according to Arnell *et al.*¹³

⁸ F. Ajzenberg and T. Lauritzen, *Revs. Modern Phys.* **27**, 77 (1955); P. M. Endt and J. C. Kluver, *Revs. Modern Phys.* **26**, 95 (1954).

⁹ Bromley, Almqvist, Gove, Letherland, Paul, and Ferguson, *Phys. Rev.* **105**, 957 (1957).

¹⁰ J. B. Gerhart, *Phys. Rev.* **109**, 897 (1958).

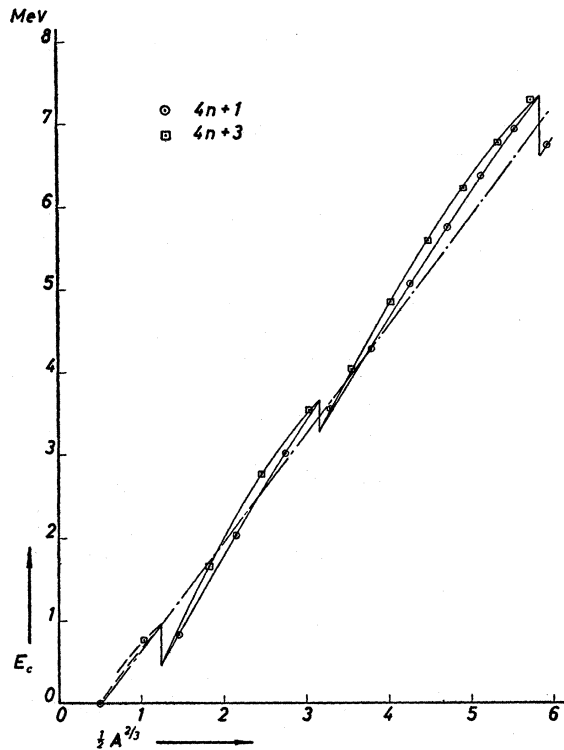


FIG. 2(a)

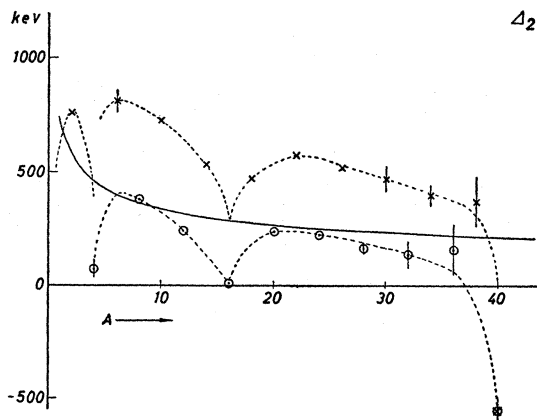


FIG. 2(b)

In the case of C^{10} the energy is very poorly known and a much better estimate may be obtained from the half-life by assuming $ft=3100$ and using the f tables of Moszkowski and Jantzen¹¹ for the E^{max} determination. The result is $E^{max}=0.927\pm 0.030$ Mev which is quite reasonable compared with the older values 1.08 ± 0.10 Mev and 0.827 ± 0.050 Mev. The weighted mean of these values is 0.912 ± 0.030 Mev, which is adopted here.

Also in the cases of Sc^{42} , V^{46} , Mn^{50} , and Co^{54} the same procedure as for C^{10} might be used but here possible branching ratios have a considerable influence on the result and the procedure is deemed too uncertain.

¹¹ S. A. Moszkowski and K. M. Jantzen, UCLA Tech. Rept. No. 10-26-55.

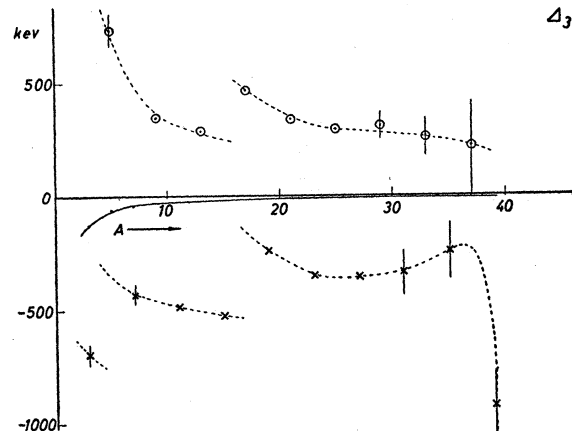


FIG. 2(c)

FIG. 2(a). Experimental Coulomb energy differences as a function of $\frac{1}{2}A^{\frac{1}{2}}$. The dotted line shows the average classical approximation. The curved lines are discussed in connection with the spheroidal model. (b) Second Coulomb energy differences Δ_2 as a function of A . Full drawn line represents expectation from formula (4). (c) Third Coulomb energy differences Δ_3 as a function of A . Full drawn line represents expectation from formula (4).

O^{15} , A^{35} , and Ca^{39} have been remeasured by Kistner *et al.*¹² The new values are used in Table I.

The values included in Table I are obtained as a best fit to the data including the corrections (7) and (8) for $4n+2$ nuclei and including 50% of the harmonic oscillator correction mentioned in connection with Eq. (19). In those cases where a detailed comparison between actual mirror nuclei E_c values and the $4n+2$ extrapolated values can be made the detailed results are given in Table II. It is seen that the agreement is good except in the case of C^{10} where no very accurate experimental E_c exist and where the value is obtained from the theoretical ft as described previously.

The values in Table I are obtained as weighted mean values of column 3 and the average of columns 4 and 5.

When the data given in Table I are plotted in a diagram of E_c vs $\frac{1}{2}A^{\frac{1}{2}}$, the results in Figs. 1 and 2 are obtained. It is interesting to note several peculiarities in this diagram.

Firstly, sharp breaks in the Coulomb energies occur at major closed shells, i.e., at $A=4, 16,$ and 40 .

Secondly, a marked difference appears between the $4n+1$ cases and the $4n+3$ cases to such an extent that it appears possible to draw separate curves for each of these cases. It is reasonable to attribute this difference to a Coulomb pairing energy difference between proton pairs.

Thirdly, two different procedures for joining the points are given in Figs. 1 and 2, respectively. In Fig. 1 straight lines are drawn through individual points inside each subshell. This procedure has been adopted by Arnell *et al.*¹³ who arrived at the possibility of breaks

¹² Kistner, Schwarzschild, and Rustad, Phys. Rev. **105**, 1339 (1957); **104**, 154 (1956) and private communication.

¹³ Arnell, Dubois, and Almén, Nuclear Phys. (to be published).

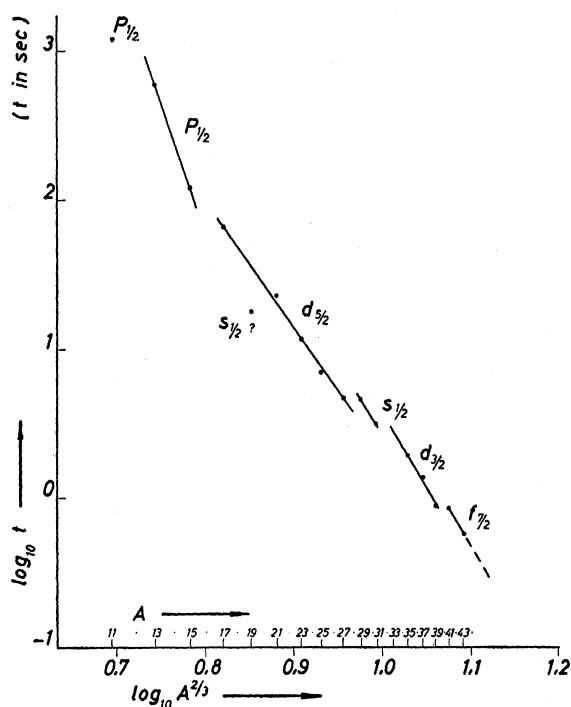


FIG. 3. Mirror decay $\log_{10} t$ as a function of $\log_{10} A^3$ according to Arnell *et al.*¹³

in the E_c values at subshell magic numbers from a study of mirror decay half-lives. They remark that these half-lives vary roughly as $(E_c^{\max})^{-5}$ so that any little deviation in E_c values will be magnified by a factor ~ 5 in the half-lives. They then plot half-lives *vs* A^3 as shown in Fig. 3 and find distinct breaks at $A=12.28$ and 32 in addition to the breaks at major shells. However, part of these effects are certainly due to the fact that t is also inversely proportional to the square of the β -decay matrix elements which varies somewhat from nucleus to nucleus. Actually, a reasonably good fit to most of the variation is obtained by comparison with the semiempirical matrix element formula given previously¹⁴

$$\left| \int \sigma \right|^2 = 4 \frac{J+1}{J} \left(\frac{\mu - g_1^J}{g_s - g_1} \right)^2, \quad (10)$$

where $\left| \int \sigma \right|^2$ is the square of the Gamow-Teller matrix element, J the nuclear spin, μ the magnetic moment, g_1 the orbital angular momentum gyromagnetic ratio for the last particle, and g_s that for the spin. The empirical $\left| \int \sigma \right|^2$ values derived from the experimental ft values¹³ and the (B, x) diagram information¹⁵ are compared with the values calculated from Eq. (10) and empirical magnetic moments in Fig. 4. The general agreement is

¹⁴ A. Winther and O. Kofoed-Hansen, Kgl. Danske Videnskab. Selskab. Mat-fys. Medd. 27, No. 14 (1953).

¹⁵ O. Kofoed-Hansen and A. Winther, Kgl. Danske Videnskab. Selskab. Mat-fys. Medd. 30, No. 20 (1956). The values $B=2820$ and $=0.545$ have been used taking into account the new O^{14} data.

quite reasonable, certainly the Ne^{19} anomaly is very clearly explained. Also, this general agreement is worth remembering for any calculations on nuclear structure in this region.

The second approach is to draw curved lines through the points between successive major shells, as in Fig. 2. In both cases, the general conclusion is that the E_c breaks at major shells constitute an appreciable effect whereas the breaks at subshells are doubtful and if they are real it must be concluded that they are very small. This is further illustrated in Figs. 2(b) and 2(c) where second and third Coulomb energy differences are given according to the definitions

$$\Delta_2(Z) = E_c(Z+1, Z) - E_c(Z, Z-1)$$

and

$$\Delta_3(Z + \frac{1}{2}) = \Delta_2(Z+1) - \Delta_2(Z).$$

Also, in these diagrams, major shell effects at $A=4.16$ and 40 are evident whereas no certain evidence for shell effects at subshells is found.

CLASSICAL MODEL

In Fig. 2 a dotted line has been drawn through the midpoints of the E_c breaks at magic numbers. The data for this line lead to the result,

$$r_0 = 1.30 \times 10^{-13} \text{ cm}, \quad (11)$$

when compared with Eqs. (4) and (6). This value is lower than the older determinations. This is simply due to the experimental accuracy being considerably improved and to the application of the modified formula (4). The result (11) is also in excellent agreement with electron scattering data in this mass region as illustrated in Fig. 5(a). It should be noted that the application of Eq. (2a) yields $r_0 = 1.47 \times 10^{-13}$ cm which is the result that has led to so much confusion when compared with electron scattering and μ -mesic atoms.

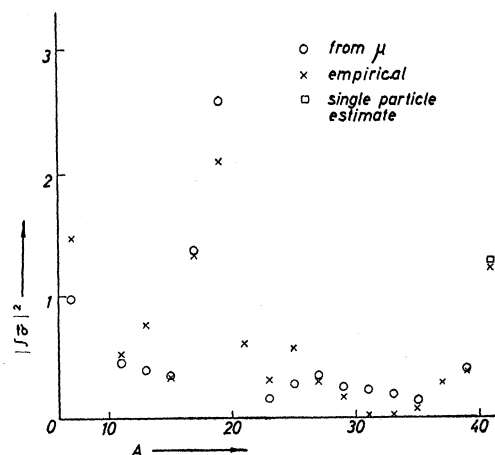


FIG. 4. Mirror decay Gamow-Teller matrix elements as a function of A .

BASIC FORMULAS FOR QUANTUM MECHANICAL APPROACH

The quantum mechanical Coulomb energies have been calculated by different authors using different models. Thus, Carlson and Talmi⁵ used the harmonic oscillator potential and Cooper and Henley³ used the infinite well. Both of these models are based on a single parameter which is then related to r_0 . Jancovici⁴ calculated for $A=15$ and 17 with a finite well and recently Sood and Green⁷ used a more detailed potential.

In all of these cases we may use the formulas for Coulomb energies given by Condon and Shortley¹⁶ from which we deduce the following equation for the Coulomb energy e^2C measured in units characteristic to the model.

$$e^2C(n, l, v) = e^2 \left\{ \sum_{\text{lower shells}} 2(2l'+1) \times [F^0(nl, n'l') + \sum_k C_{ll'k} \cdot G^k(nl, n'l')] + v \left[F^0(nl, nl) + \frac{2l+1}{4l+1} \sum_{k>0} C_{ll'k}^{mm'} F^k(nl, nl) \right] \right\} \quad (12)$$

for the Coulomb energy of the $(v+1)$ th proton in the n, l shell and where the integrals F^k are given by

$$F^k(nl, n'l') = e^2 \int_0^\infty \frac{1}{r_2^{k+1}} R_{nl}^2(r_2) \int_0^{r_2} r_1^k R_{n'l'}^2(r_1) dr_1 dr_2 + e^2 \int_0^\infty \frac{1}{r_2^{k+1}} R_{n'l'}^2(r_2) \int_0^{r_2} r_1^k R_{nl}^2(r_1) dr_1 dr_2, \quad (13)$$

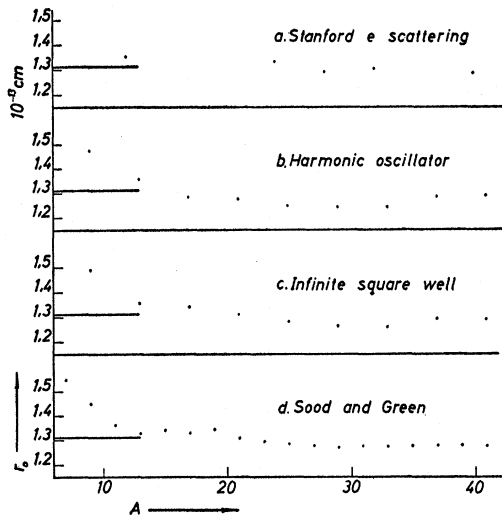


FIG. 5. Radius constant r_0 as a function of A for different methods of determination.

¹⁶ E. U. Condon and G. H. Shortley, *The Theory of Atomic Spectra* (Cambridge University Press, New York, 1935), p. 177 ff.

where $R_{nl}(r)$ is the normalized radial wave function for a particle in the nl shell. Similarly the integrals G^k are given by

$$G^k(nl, n'l') = 2e^2 \int_0^\infty \frac{1}{r_2^{k+1}} R_{nl}(r_2) R_{n'l'}(r_2) \int_0^{r_2} r_1^k R_{nl}(r) \times R_{n'l'}(r_1) dr_1 dr_2. \quad (14)$$

The coefficients $C_{ll'k}^{mm'}$ are geometrical factors which depend on the angular momentum coupling scheme. In some of the following calculations we use the simple approach of assuming an equal sharing of each single particle in this contribution as it may be calculated for a complete shell, i.e., assume independence of mm' . In this case the $C_{ll'k}^{mm'}$ may be found directly from tables in Condon and Shortley. It should be noted that l' and k must fulfill a triangle relation.

It is also necessary to calculate the equivalent sphere radius which is given by

$$B^2(n, l, v) = \frac{5}{3A} \left[\sum_{\text{lower shells}} 4(2l'+1) \int_0^\infty r^2 R_{n'l'}^2 dr + (2v+1) \int_0^\infty r^2 R_{nl}^2 dr \right], \quad (15)$$

again in units appropriate to the model applied.

Expressing B as

$$B(n, l, v) = r_0 A^{\frac{1}{3}}, \quad (16)$$

we see that

$$E_c(Z+1, Z) = \frac{C(n, l, v) B(n, l, v) e^2}{A^{\frac{1}{3}} r_0}, \quad (17)$$

where e^2/r_0 is an energy unit and where (17) has a form similar to (4). Here, the relation between Z and v for mirror nuclei is given by

$$v = Z - \sum_{\text{lower shells}} 2(2l'+1). \quad (18)$$

Furthermore, if we want to use the $A=4n+2$ nuclei then our correction factor given in Eqs. (7) and (8) must be replaced by

$$E_c^{4n+2} \left(\frac{A^{4n+2}}{A^{\text{mirror}}} \right)^{\frac{1}{3}} \left(\frac{B^{\text{mirror}}}{B^{4n+2}} \right), \quad (19)$$

which leads to the last column in Table II where calculations have been made for the harmonic oscillator and finally in Table I the $4n+2$ data have been included with 50% of the harmonic oscillator contribution which seems more realistic if one compares with B variations in more reasonably models like that applied by Sood and Green.⁷ Finally, if r_0 varies appreciably from $A=4n+2$ to the mirror nucleus this has to be taken into account. Only in the case of C^{10} is the effect appreci-

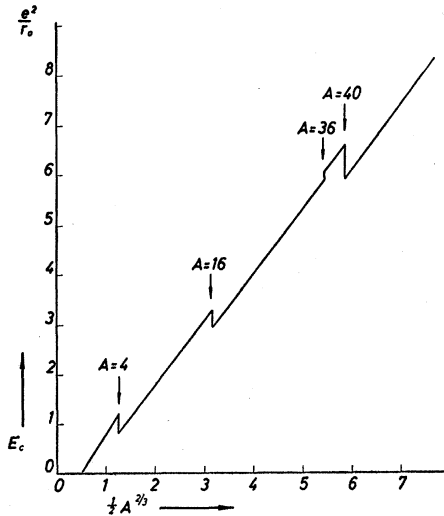


FIG. 6. Harmonic oscillator E_c values in units e^2/r_0 as a function of $\frac{1}{2}A^{\frac{1}{2}}$.

able and would actually account for most of the deviation found in Table II in this case.

HARMONIC OSCILLATOR AND INFINITE WELL

In both the harmonic oscillator and the infinite well the essential model parameter is eliminated from our Coulomb energies by forming the expression (17). In the harmonic oscillator the parameter is the frequency ω and in the infinite well the parameter is the well radius ρ . If the simple assumption of averaging over closed shells is used, it is easy to carry out the calculations of B and C and for the harmonic oscillator. All integrals can be given in closed form in a simple manner by applying the equation

$$\begin{aligned}
 F_{m,n}(\beta,\gamma) &= \int_0^\infty r_1^{2m+1} \exp(-\beta r_1^2) \int_0^{r_1} r_2^n \exp(-\gamma r_2^2) dr_2 dr_1 \\
 &= (-1)^{m+n} \frac{\partial^m}{\partial \beta^m} \frac{\partial^n}{\partial \gamma^n} \int_0^\infty r_1 \exp(-\beta r_1^2) \int_0^{r_1} \exp(-\gamma r_2^2) dr_2 dr_1 \\
 &= (-1)^{m+n} \frac{\partial^m}{\partial \beta^m} \frac{\partial^n}{\partial \gamma^n} \left[\frac{\sqrt{\pi}}{4} \left(\frac{1}{\beta} \frac{1}{(\beta+\gamma)^{\frac{1}{2}}} \right) \right]. \quad (20)
 \end{aligned}$$

The results for the harmonic oscillator are shown in units e^2/r_0 in Fig. 6 with the rather arbitrary order of filling of the shells of $1s$, $1p$, $1d$, $2s$, and $1f$. It is evident that this model yields major breaks at magic numbers $A=4$, 16 , and 40 . Exactly the same results are obtained when the square well potential is used.⁶ In both cases r_0 values may be obtained by individual comparison with the experimental Coulomb energies. The results are given in Figs. 5(b) and 5(c).

In both cases also the resultant E_c curves as a function of $\frac{1}{2}A^{\frac{1}{2}}$ are very nearly straight lines for a fixed

value of l . Thus, none of these models explains the possible curvature indicated in Fig. 2.

HARMONIC OSCILLATOR WITH DETAILED COUPLING SCHEMES

Carlson and Talmi⁵ have carried out a careful analysis of the results to be expected from a harmonic oscillator potential assuming jj coupling and LS coupling. Using Feenberg and Goertzel's² expression for the Coulomb energy

$$E_c(Z+1, Z) = aZ + \frac{1}{2}[1 + (-1)^{Z+1}]b. \quad (20a)$$

Carlson and Talmi determine the magnitude $x = (a-b)/(a+b)$ from theory. For the states of lowest proton seniority in jj coupling they find $x=0.55$. With LS coupling and lowest proton seniority their result is 0.44 whereas averages over all states of the same proton spin in LS coupling leads to $x=0.83$. Experimentally, we may find the second differences $E_c(Z+1, Z) - E_c(Z, Z-1) = \Delta_2(Z) = a + (-1)^{Z+1}b$ which split into two relatively smooth curves [see Fig. 2(b)] when the new data are used and from these curves determine $(a-b)/(a+b)$. The results of this procedure is <0.5 in reasonable agreement with theory. A detailed variation through each major shell is evident and actually $(a-b)/(a+b) \rightarrow 0$ near major shells and here ~ 100 kev of the $4n+1$, $4n+3$ effect is unaccounted for by the detailed calculations.

HARMONIC OSCILLATOR WITH SPIN-ORBIT INTERACTION

If we add an $l \cdot s$ interaction to the harmonic oscillator a splitting occurs between the $l \pm \frac{1}{2}$ states in the well-known fashion. We may treat the effect by adjusting the harmonic oscillator ω appropriately so as to account in each case for this effect; i.e., we may take the effect of the spin-orbit interaction into account by introducing frequencies $\omega(n, l, j)$ which are close to the original ω but accounts for the amount of the splitting. If this is done we may still use our formulas with a

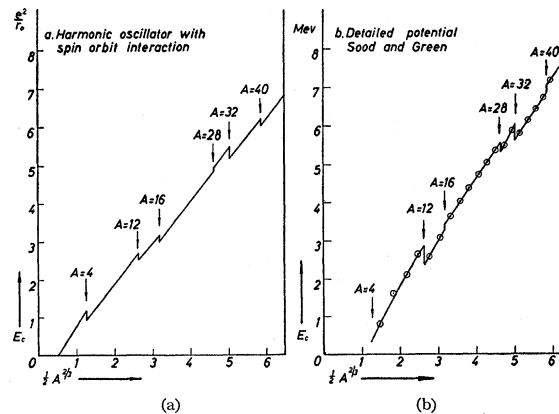


FIG. 7(a). Same as Fig. 6 but including spin-orbit interaction. (b) E_c values as a function of $\frac{1}{2}A^{\frac{1}{2}}$ as calculated by Sood and Green.⁷

slightly changed interpretation of shells and also formula (20) for the radial integrals. The result of this procedure is shown in Fig. 7(a) again in units e^2/r_0 and now with the sequence of shells $1s_{1/2}$, $1p_{3/2}$, $1p_{1/2}$, $1d_{5/2}$, $2s_{1/2}$, $1d_{3/2}$, and $1f_{7/2}$. The magnitude of the splitting has been adjusted so that the combined movements of the $f_{5/2}$ shell and the $g_{9/2}$ shell equals $\frac{2}{3}\hbar\omega$ which seems reasonable in order to account for the closed shell effect at Z and N equal to 50.

The breaks at subshells are clearly much too large compared with the experimental data although their appearance supports the general idea of subshell breaks put forward by Arnell *et al.*¹³

DETAILED POTENTIAL WELL

In a recent article Sood and Green⁷ have applied a model with the single particle potential

$$\left. \begin{aligned} V(r) &= -V_0 & \text{for } r < a \\ V(r) &= -V_0 \exp[-(r-a)/d] & \text{for } r > a. \end{aligned} \right\} \quad (21)$$

They have furthermore used a spin-orbit interaction of the Thomas form but 45 times larger in order to account for the empirical spin-orbit splitting. Also the effect of the Coulomb interaction on the wave functions is introduced. The potential is so adjusted that a varies with A as $a = (1.32A^{1/3} - 0.8) \times 10^{-13}$ cm and V_0 is taken as 45 Mev and $d = 10^{13}$ cm. These values are used in order to get agreement with experimental binding energies for $11 \leq A \leq 39$.

In order to calculate Coulomb energies a charge density in this potential of the form

$$\left. \begin{aligned} \rho(r) &= \rho_0 & \text{for } r < a \\ \rho(r) &= \rho_0 \exp[2(r-a)/d] & \text{for } r > a \end{aligned} \right\} \quad (22)$$

is assumed with total charge Z . The potential V_c of this distribution is calculated from classical theory. A single particle wave function ψ is then obtained for the $(Z+1)$ th proton and the magnitude

$$\langle \psi | V_c | \psi \rangle \quad (23)$$

is calculated.

Next, the effect of the exchange integrals is calculated using the harmonic oscillator potential essentially as described here and the result is applied as a correction to Eq. (23). The results for E_c are given in Fig. 7(b). Also the radii obtained by Sood and Green with this procedure are given in Fig. 5(d).

Sood and Green draw the important conclusion that there is no need to introduce a difference between the proton and neutron nuclear potential for the region of mirror nuclei, i.e., that there is no need for the so-called proton potential anomaly in this mass region.

However, as regards the detailed shell systematics in the mirror nuclei E_c values, the model is clearly ineffective, giving much too large subshell breaks and even major shell breaks of the wrong sign when pictured as in Fig. 7(b).

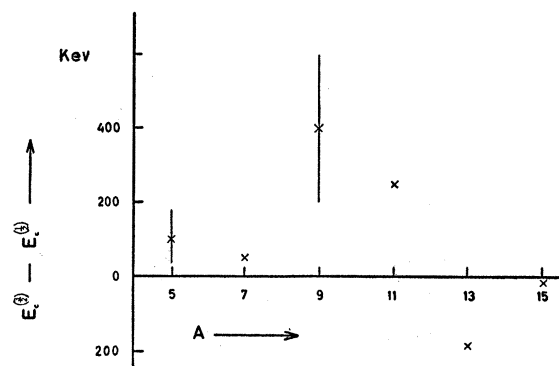


FIG. 8. The Coulomb energy difference between the lowest lying spin $\frac{1}{2}$ and $\frac{3}{2}$ states in the p shell.

SPHEROIDAL MODEL

If the nuclear deformations occurring between closed shells be taken into account the first approach leads to the nuclear Coulomb energy given by Bohr and Wheeler¹⁷

$$E_c = -\frac{3Z^2e^2}{5R_0} \left[1 - \frac{5}{36} \left(\frac{Q_0}{ZR_0^2} \right)^2 + \dots \right] \quad (24)$$

as compared with Eq. (2). Here R_0 is the radius of the sphere of the same volume as the spheroid and Q_0 is the intrinsic quadrupole moment of the nucleus. For the nuclei of largest Q_0 in the d shell this might give rise to a correction of the order -30 keV. This is smaller than the effects we are looking for.

The extra term in (24) may be considered a second order term in Q_0 . If the Bohr-Mottelson model¹⁸ is applied also, a first-order term appears from the specific coupling of the last proton to the deformed nucleus. This is of the form

$$E_c = \int \rho(r) r^2 P_2(\cos\vartheta) dV \int \frac{1}{r'^3} \rho'(r') P_2(\cos\vartheta') dV', \quad (25)$$

where ρ is the charge distribution of the last nucleon and ρ' that of the deformed core. A rough estimate of (25), valid for strong deformations, may be obtained by application of the asymptotic wave functions,¹⁹ which also have been used quite successfully by Rakavy²⁰ for the comparison of levels of nuclei in the beginning of the d shell. Neglecting higher order terms (25) reduces to

$$E_c = \frac{1}{4} Q_0 \frac{e^2}{R_0^5} (3n_z - N) \frac{\hbar}{M\omega}$$

in the notation used in references 19 and 20. From Eq. (15) we find $\hbar/M\omega = R_0^2/B^2$ and, consequently, for $A=23$ we obtain the results $E_c = 110$ keV using the

¹⁷ N. Bohr and J. A. Wheeler, Phys. Rev. 56, 426 (1939).

¹⁸ A. Bohr and B. R. Mottelson, Kgl. Danske Videnskab. Selskab. Mat-fys. Medd. 27, No. 16 (1953).

¹⁹ S. G. Nilsson, Kgl. Danske Videnskab. Selskab. Mat-fys. Medd. 29, No. 16 (1955).

²⁰ G. Rakavy, Nuclear Phys. 4, 375 (1957).

data given in reference 20. A more detailed calculation giving similar results has been carried out by Mottelson.²¹

UNCERTAINTIES IN THE r_0 DETERMINATIONS

It is evident from the model calculations indicated here that rather large unexplained effects are present in the empirical E_c values.

The $4n+1$, $4n+3$ effect amounts to as much as 250 kev of this only 150 kev have been obtained in single particle models.

From simple models including spin orbit interaction E_c breaks at subshells of ~ 300 kev are expected the maximum observed at subshells could be ~ 150 kev but the effect is not at all well established.

²¹ B. Mottelson (private communication).

The estimate of quadrupole effects leads to a possible contribution of ~ 100 kev to E_c . This is a rough estimate and does not take into account change in the quadrupole moment due to the added charge.

So far we have considered ground states only. In the p shell the experimental data permits an estimate of the Coulomb energy difference between the lowest $\frac{3}{2}$ and $\frac{1}{2}$ states. The results are indicated in Fig. 8, roughly speaking an effect of the order ± 200 kev is observed.

There is no doubt that more refined theories will explain all of these small effects, but at present I think we ought to consider them uncertainties and state that a reliable result from mirror nuclei Coulomb energies can be expressed as

$$r_0 = (1.28 \pm 0.05) \times 10^{-13} \text{ cm.}$$

Nuclear Matter Distributions from Coherent Neutral Pion Production*

J. E. LEISS AND R. A. SCHRACK

National Bureau of Standards, Washington 25, D. C.

INTRODUCTION

ONE of the modes in which neutral mesons can be photoproduced from nuclei is the so-called "elastic" production in which the target nucleus recoils as a whole in its ground state. This coherent production may be used to determine nuclear radii. Since the π^0 production from neutrons and protons is essentially the same, what is measured is the distribution of nuclear matter as distinct from the electric charge distribution measured in electron scattering experiments.

Previous measurements¹⁻⁴ have shown the coherent production to be a major contribution to the photoproduction. Goldwasser¹ pointed out that in helium the elastic production has a threshold about 20 Mev lower than other modes and demonstrated that the production of π^0 's in helium occurs largely in this elastic mode at low energies. Due to the high thresholds for (γ, p) and (γ, n) reactions this should also be true in carbon. Measurements at higher energies by the Massachusetts Institute of Technology group^{2,3} indicate that the elastic production is still a predominant effect in photoproduction by 250 Mev photons, although the amount

of inelastic production and of internal absorption of the mesons before leaving the nucleus is not clear.

It is desirable to study the coherent production in an energy region where absorption and scattering of the outgoing mesons as well as inelastic π^0 production will be small effects. This is clearly the region near the production threshold. For carbon, if we neglect the possibility of leaving the nucleus in an excited state, the energetic threshold for inelastic production is about 152 Mev compared to a threshold for elastic production of 135.6 Mev. Consideration of barrier effects, internal momentum distributions and the energy dependence of the π^0 cross section make it unlikely that the inelastic cross section will be an appreciable contribution even at 180 Mev. This supposition is borne out by this experiment.

An idea of the effects of meson absorption can be gained from Fig. 1 taken from Tenney and Tinlot.⁵ This is a plot of the mean free path for absorption in nuclear matter as a function of meson energy from charged meson scattering experiments. For carbon, on which our measurements have been made, and for meson energies of less than 40 Mev, the nucleus should be quite transparent, effects due to absorption being less than 20%. We thus assume that to the accuracy of the work we are reporting, this absorption might be neglected. For a spin zero element the results of a Born

* This work supported by the U. S. Atomic Energy Commission.

¹ Goldwasser, Koester, Jr., and Mills, *Phys. Rev.* **95**, 1692 (L) (1954).

² G. De Soussure and L. S. Osborne, *Phys. Rev.* **99**, 843 (1955).

³ Osborne, Barringer, Maunier, *Mass. Inst. Technol. Progress Report*, February 29, 1956. *Proceedings of Cern Symposium on High Energy Accelerators and Pion Physics* (June, 1956), Vol. 2, p. 282.

⁴ J. E. Leiss, *Bull. Am. Phys. Soc. Ser. II*, **2**, 6 (1957).

⁵ F. H. Tenney and J. Tinlot, *Phys. Rev.* **92**, 974 (1953).